Journal of Applied Mechanics Vol.10, pp.749-756 (August 2007) JSCE

Comparison of numerical wave models of long distance tsunami propagation – An application to Indian Ocean Tsunami in 2004 -

Alwafi Pujiraharjo* and Tokuzo Hosoyamada**

* M. Eng. Dept. of Civil and Envt. Eng. Nagaoka Univ. of Tech. (1603-1 Kamitomioka, Nagaoka, Niigata)
** Dr. of Eng. Associate Prof. Dept. of Civil and Envt. Eng. Nagaoka Univ. of Tech. (1603-1 Kamitomioka, Nagaoka, Niigata)

Numerical simulation of Tsunami propagation has been carried out based on four algorithms of wave dynamical equation. Besides non-linear shallow water equation which is common for the simulation, dispersive wave model (i.e. Boussinesq-type equations) is a challenge to make more reasonable model while taking care of the low computation cost. This paper discussed numerical simulation results of tsunami propagation model based on dispersive and non-dispersive models. Satellite image data is used to compare the numerical results with real field sea levels data of tsunami. Simulation results show that the dispersive models give better prediction but still need high computation cost while non-dispersive one give consistent result.

Key Words: *tsunami, Boussinesq models, nonlinear, dispersion.*

1. Introduction

Tsunami is very common coastal wave problems in earthquake-prone countries, causing devastating damages in coastal area. The Indian Ocean Tsunami 26 December 2004 is the most devastating tsunami recorded in history causing over than 200,000 deaths and millions homeless people, uncounted property and infrastructure damaged along the coasts of Indonesia, Thailand, Sri Lanka, and the Maldives. Traveling distance of tsunami vary from hundreds to thousands km around ocean basin. Prediction of tsunami arrival time is crucially important to protect the problems and for the people to evacuate. Numerical studies have been carried out to simulate tsunami propagation and several numerical methods have been proposed to enhance the numerical accuracy. Dispersive wave equation such as Boussinesq-type wave model is an example and sometimes applied to simulate coastal waves in nearshore region.

The accuracy of simulation of wave propagation around the ocean basin is important to give better prediction of ocean and coastal process. To obtain an accurate prediction, the model equations would have to include, among other things, refraction, diffraction, nonlinear shoaling, wave-wave interaction, breaking and runup treatment, etc (Kennedy et al.[6]). Navier-Stokes equations are available to do this but it is still impractical to perform a full solution of Navier-Stokes equations over many significant domains especially for tsunami propagation. Various extended Boussinesq-type equations are the one candidate of approximate models which is available to simulate wave propagation from relatively deep to shallow water.

During the last two decades, modeling wave propagation using Boussinesq-type equations is the most interesting research in the coastal modeling community. Many improvements have been documented for both of availability and capability of the models. Modeling schemes based on Boussinesq-type equations coupled with innovative extension to the theoretical framework have been shown to be accurate and revealing predictors of a wide range of near shore hydrodynamic behavior. The recent development in the field of Boussinesq models was triggered by the increasing availability of faster computer resources needed to run the models and the development of variants of the theory which could be optimized to obtain better dispersion properties thus allowing the models to treat a larger range of water depths.

Recently, a rapidly growing area of Boussinesq models application is modeling of tsunami generation, propagation and runup which in the past has traditionally been approach using models based on nonlinear shallow water equations (NLSW). At least three advantages of using Boussinesq models rather than NLSW model: first, horizontal velocity profile over the depth is

no longer constraint as constant value and vertical accelerations are no longer be neglected, second, better prediction of wave crest geometry and propagation over complex topography, and third, better frequency dispersion effects in ocean basin. In other side, Horillo et al.[3] noted that for practical purpose the NLSW model are quite reliable because the model gives consistent results compared to nonlinear Boussinesq model and full nonlinear Navier-Stokes model. Moreover the NLSW model has very low computation cost.

This paper will discuss comparisons of numerical calculation results of models based on linear shallow water (LSW) model, NLSW model, weakly nonlinear dispersive Boussinesq model (WNLB), and fully nonlinear but weakly dispersive Boussinesq model (FNLB), especially for long distance tsunami propagation. The models were applied to simulate the Indian Ocean Tsunami 26 December 2004. The tsunami source function is taken from Kowalik et al.[8]. To investigate long distance tsunami propagation, several observation data of maximum amplitude and arrival time around Sri Lanka were used to compare the numerical results. According to Kulikov[9] who reported that the tsunami wave propagation of the Indian Ocean Tsunami across southwestward of Indian Ocean were noticeably dispersive, the dispersion effects were also discussed by comparing the results of non-dispersive models (LSW and NLSW) which ignores the effects of wave dispersion and the results of dispersive models (FNLB and WNLB). The spatial and temporal distributions of the free surface at the selected points and transects as shown in Fig.1 were also discussed.

2. Model equations

Lynett and Liu[10] have been derived variant of Boussinesq models for fully nonlinear weakly dispersive waves generated by a seafloor movement. The equations are used as governing equations. The model equations are written in terms of $\mathbf{u}_\alpha$ and η in a non-dimensional form as

$$\frac{h_t}{\varepsilon}+\eta_t+\nabla\cdot\left((h+\varepsilon\eta)\mathbf{u}_\alpha\right)$$
$$-\mu^2\nabla\cdot\left\{(h+\varepsilon\eta)\left[\left(\tfrac{1}{6}\left(\varepsilon^2\eta^2-\varepsilon\eta h+h^2\right)-\tfrac{1}{2}z_\alpha^{\,2}\right)\nabla\left(\nabla\cdot\mathbf{u}_\alpha\right)\right.\right. \quad (1)$$
$$\left.\left.+\left(\tfrac{1}{2}(\varepsilon\eta-h)-z_\alpha\right)\nabla\left(\nabla\cdot(h\mathbf{u}_\alpha)+\frac{h_t}{\varepsilon}\right)\right]\right\}=O(\mu^4)$$

$$\mathbf{u}_{\alpha t}+\varepsilon\mathbf{u}_\alpha\cdot\nabla\mathbf{u}_\alpha+\nabla\eta$$
$$+\mu^2\left\{\tfrac{1}{2}z_\alpha^2\nabla(\nabla\cdot\mathbf{u}_\alpha)+z_\alpha\nabla\left(\nabla\cdot(h\mathbf{u}_\alpha)+\frac{h_t}{\varepsilon}\right)\right\}_t$$
$$+\varepsilon\mu^2\left\{\left(\nabla\cdot(h\mathbf{u}_\alpha)+\frac{h_t}{\varepsilon}\right)\nabla\left(\nabla\cdot(h\mathbf{u}_\alpha)+\frac{h_t}{\varepsilon}\right)\right.$$
$$-\nabla\left(\eta\left(\nabla\cdot(h\mathbf{u}_\alpha)_t+\frac{h_{tt}}{\varepsilon}\right)\right)$$
$$+\left(\mathbf{u}_\alpha\cdot\nabla z_\alpha\right)\nabla\left(\nabla\cdot(h\mathbf{u}_\alpha)+\frac{h_t}{\varepsilon}\right)$$
$$\left.+z_\alpha\nabla\left(\mathbf{u}_\alpha\cdot\nabla\left(\nabla\cdot(h\mathbf{u}_\alpha)+\frac{h_t}{\varepsilon}\right)\right)\right.$$
$$\left.+z_\alpha\left(\mathbf{u}_\alpha\cdot\nabla z_\alpha\right)\nabla\left(\nabla\cdot\mathbf{u}_\alpha\right)+\tfrac{1}{2}z_\alpha^2\nabla\left(\mathbf{u}_\alpha\cdot\nabla\left(\nabla\cdot\mathbf{u}_\alpha\right)\right)\right\} \quad (2)$$
$$+\varepsilon^2\mu^2\nabla\left\{-\tfrac{1}{2}\eta^2\nabla\cdot\mathbf{u}_{\alpha t}-\eta\mathbf{u}_\alpha\cdot\nabla\left(\nabla\cdot(h\mathbf{u}_\alpha)+\frac{h_t}{\varepsilon}\right)\right.$$
$$\left.+\eta\left(\nabla\cdot(h\mathbf{u}_\alpha)+\frac{h_t}{\varepsilon}\right)\nabla\cdot\mathbf{u}_\alpha\right\}$$
$$+\varepsilon^3\mu^2\nabla\left\{\tfrac{1}{2}\eta^2\left[\left(\nabla\cdot\mathbf{u}_\alpha\right)^2-\mathbf{u}_\alpha\cdot\nabla\left(\nabla\cdot\mathbf{u}_\alpha\right)\right]\right\}=O\left(\mu^4\right)$$

where $\mathbf{u}_\alpha = (u_\alpha, v_\alpha)$ is horizontal velocity vector at arbitrary level z_α which recommended to be evaluated at $z_\alpha = -0.531h$ (Nwogu[11]), $\nabla = (\partial/\partial x, \partial/\partial y)$ is horizontal gradient operator, while h and η are still water depth and free surface displacement, respectively. Subscript t denotes partial derivative with respect to time t. Two important parameters ε and μ are the measures of nonlinearity and frequency dispersion defined by

$$\varepsilon = a_0'/h_0', \quad \mu = h_0'/\ell_0' \quad (3)$$

where a_0', h_0', and ℓ_0' denote the dimensional form of wave amplitude, still water depth, and wave length, respectively.

Equations (1) and (2) are the full equations used in this simulations which are basically similar to the fully nonlinear weakly dispersive Boussinesq-type equations of Wei et al.[16] (FNLB) with the seafloor displacement terms were added into the equations. Truncation of the nonlinear dispersive terms of equation (1) and (2) at $O(\varepsilon^2)$ will reduce the model equations into extended Boussinesq-type equations of Nwogu (WNLB). Truncation of the dispersive terms of equation (1) and (2) at order $O(\mu^2)$ will reduce the equations into NLSW in which $\mathbf{u}_\alpha$ is the depth averaged velocity vector, while truncation of the nonlinear terms of NLSW model will reduce the model equations into LSW model.

3. Tsunami source

The Indian Ocean tsunami is mainly generated by static seafloor displacement. Kowalik et al.[8] had estimated a permanent vertical floor displacement that was calculated using static dislocation formulae of Okada[12]. The seafloor displacement calculation of Kowalik et al.[8] then was used in this model as tsunami source. The tsunami source parameters for Okada's formulae are fault location, depth, dip, strike, slip, length, and width, seismic moment, and rigidity. The fault segment is split into two segments i.e. southern and northern fault segments to

Table 1 Fault parameters used to generate seafloor movement

Earthquake parameters	Southern fault segment	Northern fault segment
Strike	335^0	350^0
Dip	8^0	8^0
Slip	110^0	90^0
Length	300 km	700 km
Depth (SW corner)	8 km	8 km
SW corner latitude	3.0 N	5.6 N
SW corner longitude	94.4 E	93.3 E
Moment	$3.2x10^{29}$ dyne cm	$7.6x10^{29}$ dyne cm
Rigidity	$4.2x10^{11}$ dyne cm^{-2}	$4.2x10^{11}$ dyne cm^{-2}

accommodate trench curvature.

The total earthquake rupture extent was calculated by using observed tsunami travel time to the northwest, east, and south of the slip zone i.e. Paradip-India, Ko Tarutao Thailand, and Cocos Island. The observed travel time then calculated and plot as reverse where the tide gauge location as the origin point. By this method, the boundary of slip rupture extent can be fully described. Strike is determined by trench orientation. Dip and slip for southern segment are based on Harvard CMT solution while slip for northern segment is set to 90^0. Rigidity is assume to be $4.2x10^{11}$ dyne cm^{-2}. The fault parameters are listed in Table 1. All of simulation in this study, the fault was calculated for the rise time 3.0 minutes.

4. Numerical calculation

The governing equations were solved using finite difference algorithm in a Cartesian grid as proposed by Wei et al.[15] which has been applied on their model named FUNWAVE[7]. The numerical calculation model is primarily a recreation of the Wei and Kirby's[15]. Structure of numerical calculation is similar to FUNWAVE, the difference exists in the added terms due to a time-dependent water depth caused by seafloor deformation and treatment of runup modeling by using slot method in which sponge layer is added at the slot region. A high order predictor-corrector scheme is used, employing a third order in time explicit Adam-Bashforth as predictor step and a fourth order in time Adam-Moulton implicit scheme as corrector step. The implicit corrector step must be iterated until a convergence criterion is satisfied. Fourth-order finite difference scheme is used to all spatial derivatives, yielding a model that is numerically accurate to order $(\Delta x)^4$, $(\Delta y)^4$ in space and order $(\Delta t)^4$ in time. For numerical model, (1) and (2) are calculated in dimensional form by taking $\varepsilon = \mu = 1$ and gravitational addition, g, to the coefficient of the leading order free surface derivative in momentum equations. Detail of the numerical scheme is referred to Wei and Kirby[15].

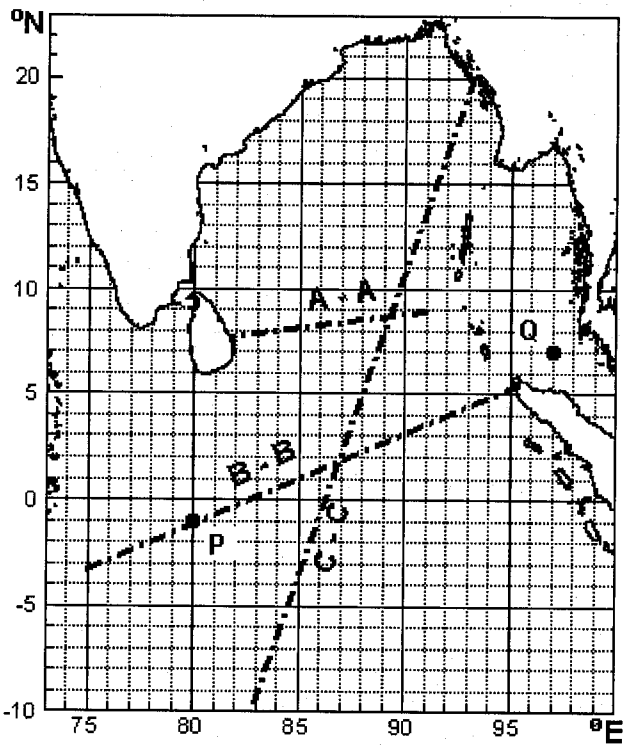

Fig. 1 Numerical domain and the location of gauges and transects.

Modified slot method of Tao as proposed by Kennedy et al.[7] and Chen et al.[1] is applied to model wave runup in which the potentially wetted grid is treated as an active part of the computational grid, while sponge layers are added at the grid which never wetted during simulation. As shown by Kennedy et al.[5], the modified slot method has better enforce of the mass conservation. Other terms e.g. eddy viscosity terms to model wave breaking, bottom friction, and sub grid-scale mixing terms are applied in the similar way as of FUNWAVE.

Numerical domain is selected around Bay of Bengal from 73^0E – 100^0E in longitude and from 10^0S – 23^0N in latitude to accommodate the satellite data comparison but minimize the grid size and achieves maximum resolution. Bathymetry is taken from ETOPO2 databank and refined into one minute resolution by linear interpolation resulting 1620x1980 of grid points with about 1.852 km x 1.852 km grid interval in the Cartesian coordinate. Compare to spherical coordinate, the Cartesian coordinate has embedded error of grid definition. The maximum error in the x direction is about 237,076 km (8.58 %) at the north part (23^O N) numerical domain and 44,052 km (1.49 %) at the south part (10^oS). While at the middle computation domain (8^oN) the error is about 27,661 km (0.93 %). It is decided to not make correction to domain error because most part of research discussion is close to the equator line. Coriolis effects is also be neglected in the numerical computation.

According to the grid resolution time interval was chosen to 2 seconds due to numerical stability of the models. Open boundary condition was specified at all ocean boundaries by adding sponge

layers at those boundaries. The mean water level specified in the models did not include the effects of tides.

During the calculations, maximum wave amplitude and tsunami arrival time was recorded at every grid point. Time series of free surfaces are also recorded at several locations, i.e. points P, Q, R, and S as shown in Fig. 1. Spatial profile of free surface along transects A–A, B–B, and C–C will also be discussed. The spatial free surface along transects C–C will be compared to the satellite recorded data of Jason 1 satellite altimetry. Transects A–A and B–B were chosen based on the fact from simulation, it is known that the main tsunami propagation are directed toward those direction i.e. Sri Lanka and Maldives.

5. Simulation results and discussion

Numerical calculations were conducted for 350 minutes (10500 time step) of tsunami propagation starting from the seafloor deformation event. Simulation results obtained by WNLB and FNLB models are not significantly different. It indicates that the non-linear dispersion terms are not give important effects for modeling of tsunami propagation. While the simulation results of LSW and NLSW models although show similarity of the wave patterns but different in the results of wave height and travel time. Because of the similarity, the next discussion will be carried out only the simulation results obtained by LSW, NLSW and WNLB models.

Although not documented here, we noted that simulation using FNLB model need a very high computation cost (about 20.5 hours by Pentium 4 processor), WNLB model is more moderate (15 hours), while LSW and NLSW models have very low computation cost (7 hours and 7.5 hours, respectively) using the same processor.

5.1 Maximum amplitude and runup

All of the models show similarity of maximum amplitude distribution. Fig. 2 shows plot of the maximum amplitude calculated by WNLB model. The figure shows that there are two main energy lobes of tsunami propagation, one directed to Sri Lanka and the other directed toward southwest i.e. Maldives. All of the models show the similarity of distribution of maximum amplitude.

The highest runup is predicted in the simulation (using WNLB model as example) near northern Sumatra (10.77 m), Thailand (15.51 m), and Sri Lanka (8.4 m). Maximum waves runup at several locations are recorded and shown in Table 2. For long distance and deep water tsunami propagation, the results of models prediction are compare to the observation results resumed in Wijetunge[1)] around Sri Lanka (seven first lines). Maximum runup at Thailand and Indonesia is also shown in Table 2 (the last three lines). It is noted that because of the coarse of grid size used in the models simulation (about 1.852 km), the gauges are not

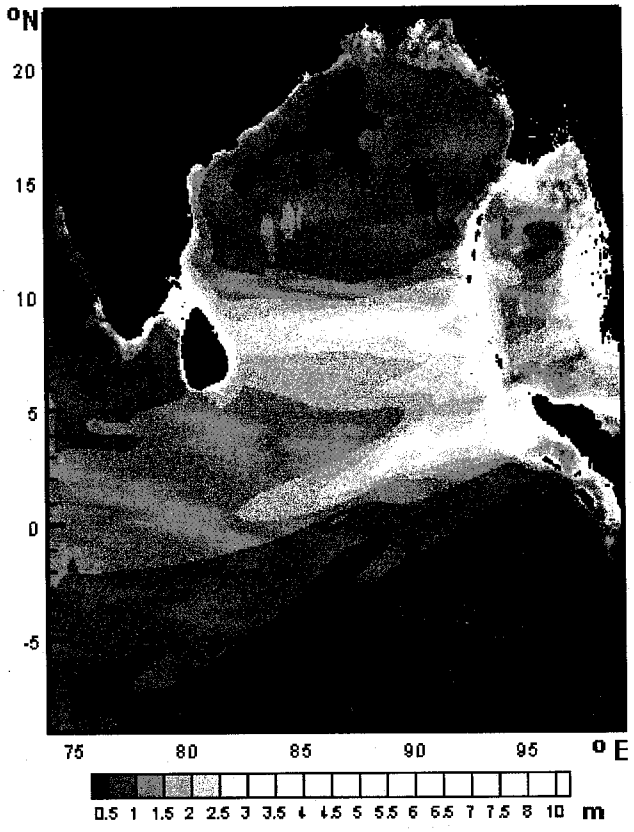

Fig. 2 Plot of maximum amplitude around numerical domain

located at exactly match with actual location All of the models show good agreement compared to the observation results, but overestimation trend is noted although in some case show underestimation caused by the coarsest of grid resolution used in simulation.

Distribution of tsunami height around Sri Lanka is not umiform caused by many factors of tsunami travel path and morphological domain. Because of these complexities, combination of both nonlinearity and dispersion give significant effects to the wave amplitude. For long distance and deep water tsunami propagation, the difference prediction between dispersive and non-dispersive models is quite significant (0.1 – 0.8 m). The significant difference also can be seen between the prediction by LSW model and NLSW model (0.02 – 0.55m).

The difference prediction between dispersive (WLNB) and non-dispersive (NLSW) models is not significant for short distance and shallow water tsunami propagation because of no enough time and space to develop the dispersive effects at this location. but it is quite significant for the different between linear model (LSW) and nonlinear models (NLSW model and WNLB model). Most of calculation results of maximum amplitude using non-dispersive (LSW and NLSW) models are greater than dispersive (WNLB and FNLB) models, it shows that during long distance propagation at the deep water, the dispersion effects will

Table 2 Maximum runup predicted by the models and observation results.

Location	Maximum runup (m)				
	Obs.	LSW	NLSW	WNLB	FNLB
Galle (80.31°E, 6.03°N)	4.0	4.68	4.70	3.88	3.87
Hambantota (80.94°E, 6.12°N)	7.0	6.97	6.42	6.78	6.78
Potuvil (81.82°E, 6.85°N)	7.2	7.23	7.18	6.58	6.58
Batticaloa (81.56°E, 7.81°N)	5.5	7.02	6.96	6.58	6.58
Kalmunai (81.73°E, 7.5°N)	7.0	8.85	8.68	8.40	8.40
Trincomalee (81.2°E, 8.6°N)	3.0	5.59	5.60	5.40	5.40
Colombo (79.84°E, 7.00°N)	3.6	3.46	3.48	3.61	3.61
Khao Phi Phi, (98.78°E, 8.85°N)	5.0	5.18	5.05	5.08	5.08
Kamala Beach, (98.28°E, 7.97°N)	4.5	2.43	2.48	2.52	2.52
Banda Aceh, Ina (95.28°E, 5.57°N)	10.5	9.89	9.81	9.72	9.72

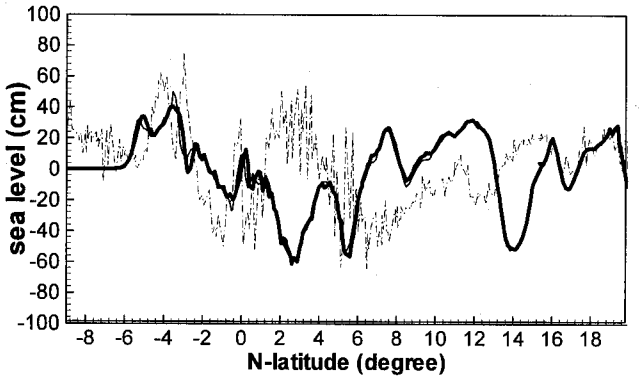

Fig. 3 Sea level along transect C–C measured by Jason 1 (dash), WNLB model (bold), and NLSW model (solid)

decrease the amplitude but expand the wavelength.

Jason 1 satellite altimetry has measured the tsunami front face in the satellite track number 129. The measured sea level for transect 109 or 2 hours after earthquake event given in Gower[2] is compared to the model simulation results (transects C–C given in Fig. 1). Fig. 4 shows comparison of sea level along transects C–C obtained by models and Jason 1's measurement. The results between WNLB model and NLSW model show similarity.

Comparisons of snap shot sea level between models result and measurement result along transect C-C shows that the front face of tsunami has the same location at that time. Similarity profile between satellite record data and model result is weak. The relatively good agreement between measured and modeled elevation occurs between 0°S–8°S in latitude. The difference shows that main energy lobe direction of tsunami propagation toward Maldives is different between the model simulation and the real condition. It means that the tsunami source needs to be improved to increase the accuracy of model simulation. Improvement could be done by modified the shape of tsunami source and the rise time of tsunami event.

5.2 Arrival time

It is important for the tsunami prediction and warning system to predict travel time of tsunami from the source region to the given location. Over prediction of tsunami arrival time is better than underestimation prediction for tsunami warning system because people will be evacuated earlier than it must be. Tsunami arrival time at each grid point is also recorded during simulation of the models. We defined tsunami arrival time as the time of the first extreme surface elevation at the gauge location.

Table 3 shows the comparison of tsunami arrival time predicted by the models at given location starting from the seafloor deformation event. Comparisons of arrival time between models prediction and observation show that all of the models over predict of tsunami arrival time. It could be seen from Table 3 that all of the model results have over prediction, more than 20 minutes at Colombo, Sri Lanka and more than 30 minutes at Taphao Noi, Thailand. The difference between model and observation results could be caused by many factors including e. g. mismatching grid point location, definition of tsunami arrival time, and tsunami source function.

At Colombo, Sri Lanka tsunami arrival time calculated by dispersive WNLB model is 0.8 minutes later compare to the result by NLSW model. The results by LSW model also shows consistency. At Taphao Noi and yacht Mercator Thailand, the calculation results of WNLB model show similarity compare to NLSW model results, while the LSW model shows inconsistent result, it means that the nonlinearity effect is important at shallow water.

5.3 Dispersion and nonlinearity effects

The dispersion effects play an important role in propagation of large-medium size tsunami. To visualize the dispersion effects, two dimension snapshot free of surface elevation at selected simulation domain is carried out. Visualization window is conducted from 80°E – 99°E and 2°S – 15.5°N. From the visualization, the wave pattern after long distance tsunami propagation can be seen. Simulation results by LSW model and NLSW model show the similarity of wave pattern, while WNLB model and FNLB model have the same results.

Fig. 4 shows snapshot image window of free surface pattern

Table 3 Tsunami arrival time predicted by the models

Location	Arrival time (minutes)			
	Obs.	LSW	NLSW	WNLB
Colombo, Sri Lanka (79.84°E, 7.00°N)	179	158.4	158.1	158.9
Taphao-Noi, Thailand (98.42°E, 7.83°N)	138	100.4	101.4	101.5
Mercator, Phuket, Thailand (98.28°E, 7.73°N)	108	101.4	100.6	100.8

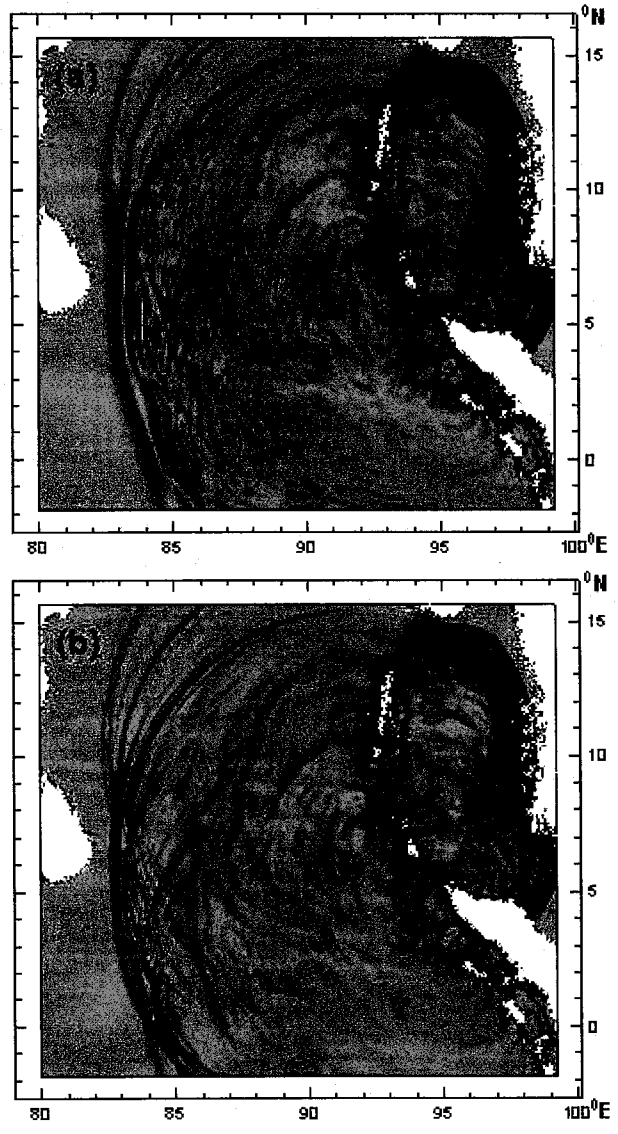

Fig. 4 Snapshot of free surface at 1h 40 min after tsunami event obtained by: (a) NLSW model, (b) WNLB model.

obtained by NLSW model and WNLB model at time 1h 40 min. At this time, tsunami reaches the eastern part of boundary in calculation domain. On the other hand, leading wave of tsunami is still traveling to India and Sri Lanka. Horizontal shape of the crest line of leading wave is very similar between two cases.

The WNLB model shows a series of wave patterns behind the leading wave due to the dispersion effects. Waves propagation which comprises multiple amplitudes and frequency components are formed behind the leading wave at the western. Tsunami sometimes takes its peak not in first arrival wave but in successive waves. Evaluation of wave dispersion is important to estimate the following waves after the first arrival wave. The dispersion effects at western of the source are greater than eastern because the water depths are also greater. It shows that the tsunami is essentially non-dispersive in shallow water. Although does not include the dispersion effects, the NLSW model shows that the wave front tip matches very well to the results of WNLB model.

To visualize more detail of the dispersion effects, comparison of temporal and spatial free surfaces between NLSW and WNLB models result were carried out at points P(80°E, 1°S) and Q(97°E, 7°N) and also along transects A – A and B – B. At the location near the source region, the dispersion effects can not be seen clearly because for short distance tsunami propagation dispersive waves do not enough time to develop. In order to show the dispersion effects clearly, the spatial profile is shown after long distance tsunami propagation. Fig. 5 shows the spatial profile of sea levels along transects A – A at 1 hour 40 minutes after seafloor deformation event. Dispersion effects are shown by WNLB model at the deep water after long distance tsunami propagation. The leading wave of tsunami is difference between the results of non-dispersive model and dispersive model. The LSW and NLSW model show similar results. The leading LSW and NLSW wave is higher and shifted forward in space compare to WNLB model results. WNLB model produces a series of waves following the leading wave. It means that after long distance propagation, tsunami will come in several peaks after the leading wave. Wavelength of the leading wave is about 180 km.

The similar trend is also showed along transects B – B. Fig. 6 shows spatial profile of sea levels along the second main energy lobe of tsunami directed into Maldives. The dispersive waves can be seen clearly by WNLB model. The leading wave with about 220 km was propagated and followed by several waves with different length and amplitude. While the non-dispersive model shows the leading wave with higher amplitude. Water level profile at the right side (near the tsunami source region) is similar between dispersive and non-dispersive model.

Fig. 7 shows temporal variation of sea level at point P(80°E, 1°S). Distance from the source to this location is about 2,778.22 km with 4,650 m water depth. At this location tsunami has arrived at 2 hours after the source event and propagated for long distance. The nonlinearity effect is not noticeably. Time series of sea level calculated by LSW and NLSW model has no significantly different. The dispersion effect is noticed very clear by WNLB model. After long distance propagation on deep water

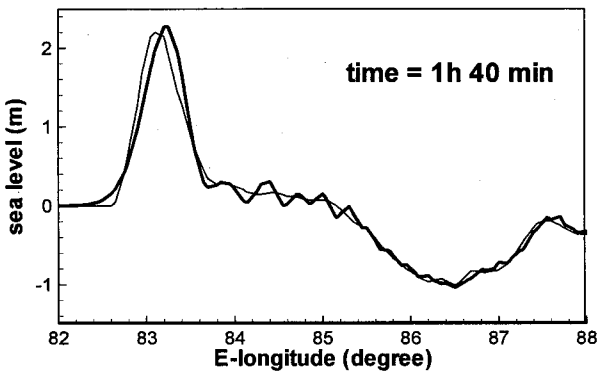

Fig. 5 Spatial sea levels along transects A-A simulated by WNLB model (bold), NLSW model (Solid), and LSW model (dashed)

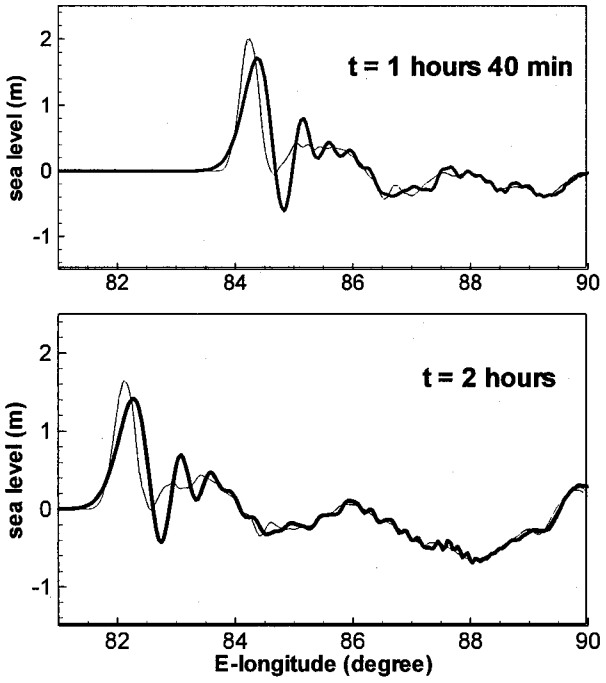

Fig. 6 Spatial sea levels along transects B-B simulated by WNLB model (bold), NLSW model (Solid), and LSW model (dashed)

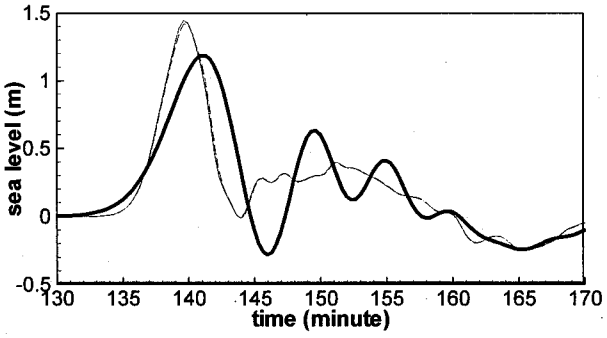

Fig. 7 Temporal sea levels at point P calculated by WNLB model (bold), NLSW model (solid), and LSW model (dashed).

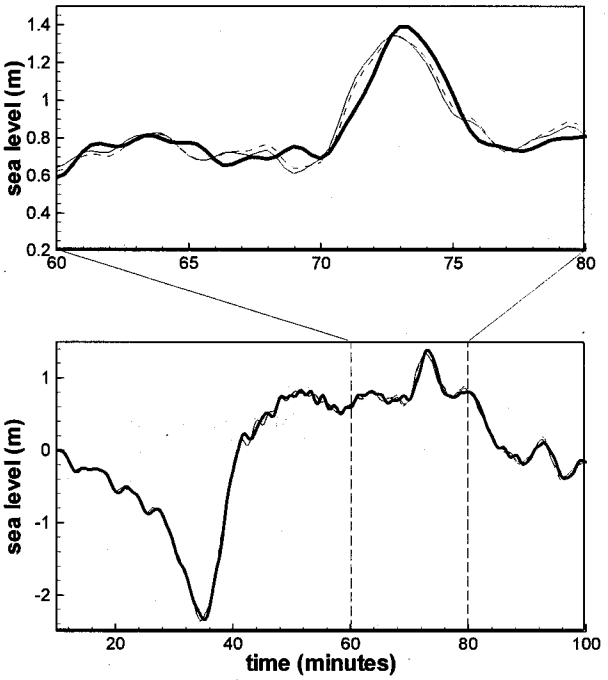

Fig. 8 Temporal sea levels at point Q calculated by WNLB model (bold),, NLSW model (solid), and LSW model (dashed).

the dispersive effect is generated. A series of waves with different period and amplitude is generated. The leading wave has about 15 minutes wave period followed by series of waves with lower period and amplitude.

Fig. 8 shows temporal variation of free surface elevation at point Q(97°E, 7°N) as given in Fig. 1 obtained by LSW model, NLSW model and WNLB model. This location is close to the source region with about 1.000 m water depth. The figure generally shows similarity of temporal variation of sea level between dispersive and non-dispersive models. Showing the figure in detail expressed the different between dispersive, non-dispersive, and non-linear model results. From the figure we can conclude that both of non-linearity and dispersion are give contribution to the wave propagation in the shallow water region.

The similarity between dispersive and non-dispersive models are caused by the location is close to the source so the dispersion effect has not enough time to develop. Moreover point Q is at shallow water in which the dispersion effect is not as high as at

deep water.

6. Conclusions

Simulation the 26 December 2004 Indian Ocean Tsunami has been conducted using four model equations. The LSW model obtained less accurate and inconsistency compared to its counterparts in predicting maximum runup and travel time because the model does not include the nonlinearity and dispersion terms but for getting the fast result for practical purpose it is quite reliable to use the LSW model. The nonlinearity and dispersion terms are important for tsunami modeling. Generally, all of the models give the similar results of tsunami propagation profile. The WNLB model produces the best results compared to its counterpart because of the accuracy and the availability to simulate the dispersion effects especially for deep water and long distance tsunami propagation. While the NLSW model is very attractive and quite reliable for practical purpose because it has low computation cost and give the consistent results compared to WNLB model.

In order to improve the accuracy of model results while still take the low computation cost, it is available for the next study to make an integrated model based on WNLB model and NLSW model in which for deep water the WNLB model is applied, while for shallow water the NLSW model is applied.

References

1) Chen, Q., Kirby, J.T., Dalrymple, R.A., Kennedy, A.B., and Chawla, A., Boussinesq modeling of wave transformation, breaking, and runup. II: 2D, *J. Waterway, Port, Coast, and Ocean Engineering*, 126(1), pp. 48-56, 2000.
2) Gower, J., Jason 1 detects the 26 December 2004 tsunami., *Eos*, Vol. 86, No. 4, 2005.
3) Horillo, J., Kowalik, Z., and Shigihara, Y., Wave dispersion study in The Indian Ocean Tsunami of December 26, 2004. *Science of Tsunami Hazards*, Vol. 25 No. 1 pp. 42–63. 2006.
4) Imamura, F., N. Shuto, and G. Goto., Numerical simulation of the transoceanic propagation of tsunamis. Congress Asian and Pacific Regional Divison, International Association for Hydraulic Research, Kyoto Japan 6. pp 265-272, 1998.
5) Ji, C. : Preliminary Result of the 04/12/26 (Mw 9.0), OFF W COAST of Northern Sumatra earthquake, posted at Http://www.gps.caltech.edu/%7Ejichen/Earthquake/2004/aceh/aceh.html.
6) Kennedy, A.B., Chen, Q., Kirby, J.T., and Dalrymple, R.A., Boussinesq modeling of wave transformation, breaking, and runup. I: 1D, *J. Waterway, Port, Coast, and Ocean Engineering*, 126(1), pp. 39-47, 2000.
7) Kirby, J.T., Wei, G., Chen, Q., Kennedy, A.B., and Dalrymple, R.A., FUNWAVE 1.0 Fully nonlinear Boussinesq wave model Documentation and User's Manual. Research Report no. CACR-98-06, Univ. of Delaware, 1998.
8) Kowalik, Z., Knight, W., Logan, T., and Whitmore, P., Numerical modeling of the global tsunami: Indonesia Tsunami of 26 December 2004, *Science of Tsunami Hazards*, Vol. 23, No. 1. pp. 40-56, 2005.
9) Kulikov, E. Dispersion of the Sumatra Tsunami Waves in the Indian Ocean detected by satellite altimetry. http://www-sci.pac.dfo-mpo.gc.ca/osap/projects/tsunami/documents/195610_0_merged_1107633516.pdf.
10) Lynett, P., and Liu, P.L.-F. : A numerical study of submarine landslide generated waves and runup, *Proc. R. Society London*, 458, pp. 2885-2910, 2002.
11) Nwogu, O., Alternative form of Boussinesq equations for nearshor wave propagation., *J. Waterway, Port, Coast, and Ocean Engineering*, 119(6), pp. 618-638, 1993.
12) Okada, Y. : Surface deformation due to shear and tensile faults in a half-space, *Bulletin of the Seismological Society of America*, 75(4), pp. 1135-1154, 1985.
13) Tao, J., Numerical modeling of wave runup and breaking on the beach. *Acta Oceanologica Sinica*, 6, pp. 93-122, 1984.
14) Watts, P., Ioualalen, M., Grilli, S., Shi. F., and Kirby, J. T., Numerical simulation of the December 26, 2004 Indian Ocean Tsunami using high-order Boussinesq model., *Fith Int. Symp. WAVES 2005*, Madrid Spain, July, 2005.
15) Wei, G., Kirby, J.T., Time-dependent numerical code for extended Boussinesq equations, *J. Waterway, Port, Coast, and Ocean Engineering*, 121(5), pp. 251-261, 1995.
16) Wei, G., Kirby, J. T., Grilli, S. T., and Subramanya, R., A fully nonlinear Boussinesq model for surface waves. Part 1. Highly nonlinear unsteady waves. *J. Fluid Mechanic.* 294. pp 71-92, 1995.
17) Wijetunge, J. J., Tsunami on 26 December 2004: Spatial distribution of tsunami height and the extent of inundation in Sri Lanka., *Science of Tsunami Hazards*, Vol. 24, No. 3. pp. 225–239 , 2006.

(Received: April 12, 2007)